

Article

Acid Solution Processed VO₂-Based Composite Films with Enhanced Thermochromic Properties for Smart Windows

Zhe Wang^{1,2}, Bin Li¹, Shouqin Tian^{1,*}, Baoshun Liu¹, Xiujian Zhao¹, Xuedong Zhou¹, Gen Tang² and Aimin Pang^{2,*}

¹ State Key Laboratory of Silicate Materials for Architectures, Wuhan University of Technology (WUT), No. 122, Luoshi Road, Wuhan 430070, China; 290952@whut.edu.cn (Z.W.); libin625@whut.edu.cn (B.L.); liubaoshun@126.com (B.L.); opluse@whut.edu.cn (X.Z.); xuedong_zhou@whut.edu.cn (X.Z.)

² Science and Technology on Aerospace Chemical Power Laboratory, Hubei Institute of Aerospace Chemotechnology, Xiangyang 441003, China; tanggen518@126.com

* Correspondence: tiansq@whut.edu.cn (S.T.); ppam@tom.com (A.P.); Tel.: +86-027-87652553 (S.T.); Fax: +86-027-87883743 (S.T.)

Abstract: As a typical thermochromic material, VO₂ coatings can be applied to smart windows by modulating the transmission of near infrared (NIR) light via phase transition. However, the inherent undesirable luminous transmittance (T_{lum}) and solar modulation efficiency (ΔT_{sol}) of pure VO₂ impede its practical application. In order to solve this problem, the porous VO₂ based composite film was prepared by magnetron sputtering and subsequent acid solution process with Zn₂V₂O₇ particles used as a sacrificial template to create pores, which showed excellent T_{lum} (72.1%) and enhanced ΔT_{sol} (10.7%) compared with pure VO₂ film. It was demonstrated that the porous structure of the film caused by acid solution process could improve the T_{lum} obviously and the isolated VO₂ nanoparticles presented strong localized surface plasmon resonance (LSPR) effects to enhance the ΔT_{sol} . Therefore, this method will provide a facile way to prepare VO₂ based films with excellent thermochromic performance and thus promote the application of the VO₂ based films in smart windows.

Keywords: VO₂; thermochromic properties; acid solution process; porous structure



Citation: Wang, Z.; Li, B.; Tian, S.; Liu, B.; Zhao, X.; Zhou, X.; Tang, G.; Pang, A. Acid Solution Processed VO₂-Based Composite Films with Enhanced Thermochromic Properties for Smart Windows. *Materials* **2021**, *14*, 4927. <https://doi.org/10.3390/ma14174927>

Academic Editor: Dirk Poelman

Received: 13 July 2021

Accepted: 23 August 2021

Published: 30 August 2021

Publisher's Note: MDPI stays neutral with regard to jurisdictional claims in published maps and institutional affiliations.



Copyright: © 2021 by the authors. Licensee MDPI, Basel, Switzerland. This article is an open access article distributed under the terms and conditions of the Creative Commons Attribution (CC BY) license (<https://creativecommons.org/licenses/by/4.0/>).

1. Introduction

VO₂ is an important thermochromic material with high potential for low-cost switching and energy saving devices which has been widely studied due to its reversible semiconductor to metal transition accompanied by a dramatic change in optical and electrical properties at near room temperature (~68 °C) [1]. With this characteristic, VO₂ was usually investigated for thermochromic smart windows to reduce building energy consumption in response to the dynamic environmental temperature since significant decrease in the NIR transmittance and negligible changes in the visible and UV transmittance upon phase transition were exhibited. Therefore, it is of great significance to prepare VO₂ based films with excellent thermochromic properties for smart windows. However, VO₂ based thermochromic window is faced with great challenges of reducing the phase transition temperature (T_c), improving durability, enhancing luminous transmittance (T_{lum}) and solar modulation efficiency (ΔT_{sol}) simultaneously. It is generally believed that the T_{lum} up to 60% and the ΔT_{sol} higher than 10% to be satisfied with the actual demand of smart windows applications [2–6].

In order to tackle the above issues, various methods have been employed such as establishing nano-composite film, multilayers and porous structures [6–17], doping [2,3,13–15] and optimization of preparation technology [10,11,18–26]. Kang et al. [13] and Jiang et al. [15] introduced Zn into VO₂ lattice, which can improve the T_{lum} and ΔT_{sol} of the film, and at the same time faded the yellow color of the film, however the unsatisfied optical properties were far from application requirement. Chen et al. [7] dispersed VO₂ nanoparticles

into thermochromic nickel-bromine-ionic liquid (Ni-Br-IL) for enhancing optical performance. The composite film demonstrated desirable optical properties: $T_{l,lum} = 65.9\%$ and $T_{h,lum} = 55.3\%$ with extraordinary ΔT_{sol} of 27.0%. Wu et al. [16] introduced mesopores into the VO₂ nanoparticles using cotton as the template by hydrothermal methods. The T_{lum} of mesoporous VO₂ nanoparticles based composite film was up to 56.0%, a larger pore size could lead to a higher luminous transmittance. It was worth noting that T_{lum} and ΔT_{sol} for application of smart windows have to exceed 60% and 10% simultaneously. However, the most of the composite films prepared by the above methods have poor repeatability, durability as well as adhesive force to glass substrate. Magnetron sputtering method exhibited advantages of high repeatability; suitability for mass production; preparing coatings with uniform density, good durability and excellent ΔT_{sol} . However, the much dense and smooth surface strongly increased the reflectance of the film, thus reducing the T_{lum} significantly. Taking appropriate approaches to increase the T_{lum} of film prepared by magnetron sputtering method is of great significance for taking full advantage of the magnetron sputtering method. According to this, Long et al. [26] used an acid solution to etch the pure VO₂ film prepared by the magnetron sputtering, forming a karst landforms-like structure to improve the modulation efficiency and visible light transmittance of the VO₂ film simultaneously. VO₂ is quite easy to react with acid so that the porous structure obtained by the etching process is uncontrollable. In addition, after the acid solution process, the phase transition temperature of the film will be probably increased due to the reduce of interfacial strain [23–25], which is usually ignored and lack of detailed discussion. Therefore, it is of great importance to develop a facile method to prepare controllable porous structure of VO₂ based film.

Inspired by this analysis, differing from directly etching pure VO₂ film, we introduce Zn₂V₂O₇ as the etching template into the VO₂ film since the Zn₂V₂O₇ possess higher activity than VO₂ in the reaction with acid, which greatly improves the targeting of acid solution process, making the porous structure preparation in the film more controllable and avoiding more VO₂ is corroded to guarantee the desirable ΔT_{sol} . In this work, Zn₂V₂O₇-VO₂ composite films were prepared by magnetron sputtering followed by post annealing method using V and ZnO targets. The acid solution processed on the VO₂ composite film aimed to generate porous structure by disposing of Zn₂V₂O₇. The content of Zn₂V₂O₇ in the composite film was adjusted to vary the porosity by changing the sputtering power of ZnO target. Consequently, porous VO₂ film obtained by acid solution treatment showed the best optical performance ($\Delta T_{sol} = 10.7\%$, $T_{lum} = 72.1\%$) when the sputtering power of ZnO target was set as 150 W. It is believed that the performance meets the requirement for application in smart windows.

2. Materials and Methods

All reagents were purchased from Sinopharm Chemical Reagent Co., Ltd. and used without further purification. The cleaned quartz glass substrate was fixed with heat-resistant tape in the magnetron sputtering vacuum chamber. V (99.95%) and ZnO (99.99%) targets were used for codeposition. Before sputtering, the vacuum chamber was evacuated to 3.0×10^{-3} Pa. Then, Ar (99.99%) was introduced into the chamber and the gas flow rate was fixed at 200 sccm. First, ZnO-V composite films were deposited through direct current magnetron sputtering of V targets at power of 90 W and radio frequency magnetron sputtering of ZnO targets simultaneously at various power. The total continuous sputtering duration of V target was 15 min while the zinc oxide target was intermittently sputtered 9 times with 30 s for each time. The detailed fabrication process of ZnO-V composite films was illustrated in Figure 1a. Finally, Zn₂V₂O₇-VO₂ composite films was achieved through post annealing the ZnO-V composite films in tube furnace. Detailly, the films were put into a tube furnace with air pressure of 1000 Pa. Ramping up the temperature to 450 °C and holding for 1 h at a rate of 5 °C/min, and then cooling down naturally. For comparison, ZnV₂O₇-VO₂ composite films with different sputtering power of ZnO were denoted as

sample a1 (60 W), b1 (90 W), S1 (120 W) and c1 (150 W), respectively, and pure VO₂ film without sputtering ZnO was also prepared.

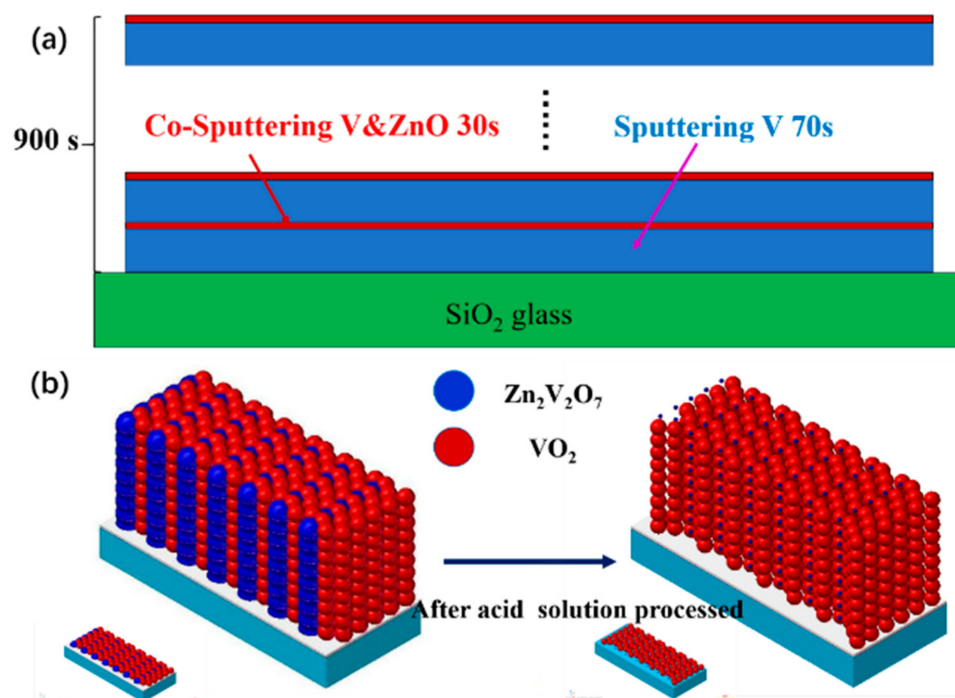


Figure 1. (a) the diagram for the ZnO-V composite film preparation process and (b) film structure before and after acid solution process.

The Zn₂V₂O₇-VO₂ composite films were put into a PTFE etching flower basket and treated in hydrochloric acid with a molar concentration of 5.6 mol/L for 5 s. After corrosion, films were quickly removed out of the acid solution and ultrasonic cleaned in deionized water and absolute ethanol for 1 min. The as-obtained porous VO₂ films were blow dried with N₂ and denoted as sample a2 (60 W), b2 (90 W), S2 (120 W) and c2 (150 W) corresponding to the Zn₂V₂O₇-VO₂ composite films respectively. The schematic diagram of films structure evolution before and after acid solution treatment were shown in Figure 1b.

Glancing-angle X-ray diffraction (GAXRD) measurements were used to characterize the crystal structure of the films on an Empyrean diffractometer (Cu K α , $\lambda = 0.154178$ nm produced under a 4kW output power, Malvern Panalytical B.V., Almelo, Netherlands). Field emission scanning electron microscope (SEM, JSM-5610LV, JEOL, Tokyo, Japan) with X-Max 50 X-ray energy spectrometer and atomic force microscopy (AFM, Nanoscope IV/Nanoscope IV, VEECO, New York, NY, USA) were adopted to observe the morphology of the films. X-ray photoelectron spectroscopy (XPS, ESCALAB 250Xi/ESCALAB 250Xi, Thermo Fisher, Waltham, MA, USA) was employed to determine the element composition of the films. An ultraviolet-visible-near-infrared spectrophotometer (UV-3600, Shimadzu, Kyoto, Japan) was used to test the solar transmittance of the films in the range of 300–2500 nm at 20 and 90 °C, respectively. The integrate T_{lum} and T_{sol} can be calculated by the following Equations (1) and (2).

$$T_{lum} = \int_{380}^{780} v_m(\lambda)T(\lambda)d\lambda / \int_{380}^{780} v_m(\lambda)d\lambda \quad (1)$$

$$T_{sol} = \int_{300}^{2500} \varphi_{sol}(\lambda)T(\lambda)d\lambda / \int_{300}^{2500} \varphi_{sol}(\lambda)d\lambda \quad (2)$$

The ΔT_{sol} can be calculated by Equation (3).

$$T_{sol} = T_{sol}(20\text{ }^\circ\text{C}) - T_{sol}(90\text{ }^\circ\text{C}) \quad (3)$$

where $T(\lambda)$ is the transmittance, λ is the wavelength of the incident light, $v_m(\lambda)$ denotes the spectral sensitivity of the light to the human eye and $\varphi_{sol}(\lambda)$ represents the irradiance spectrum of the sunlight at an atmospheric mass of 1.5 (corresponding to the sun from the horizon 37°) [27–37].

3. Results and Discussion

3.1. Structures of the Films before and after Acid Solution Treatment

The XRD patterns of the samples before (sample S1) and after (sample S2) the acid solution process as well as the pure VO₂ film were shown in Figure 2 (and Figure S1). It can be seen that sample S1 was consist of VO₂(M) and Zn₂V₂O₇ corresponding to the standard JCPDS card No. 44–252 and 28–1492, respectively. This indicates that ZnO-V composite films were fully transferred to Zn₂V₂O₇-VO₂ composite films with a reaction of ZnO and VO₂. Besides, the relative intensity of the VO₂ diffraction peaks in the Zn₂V₂O₇-VO₂ composite film were lower than those in the pure VO₂ film, implying that some of the VO₂ was consumed upon the reaction. After acid solution process, only diffraction peaks of VO₂ were observed in sample S2 and the relative intensity decreased, which indicated that Zn₂V₂O₇ as the template were totally corroded. It was worth noting that the relative intensity of VO₂ diffraction peaks remained unchanged. Consequently, porous structures could be formed through sacrifice of some Zn₂V₂O₇ particles as expected. In addition, there is a shift in the peak position of the (011) reflection of M-VO₂ among sample S1, S2 and pure VO₂ film, indicating that there are some strains in the samples.

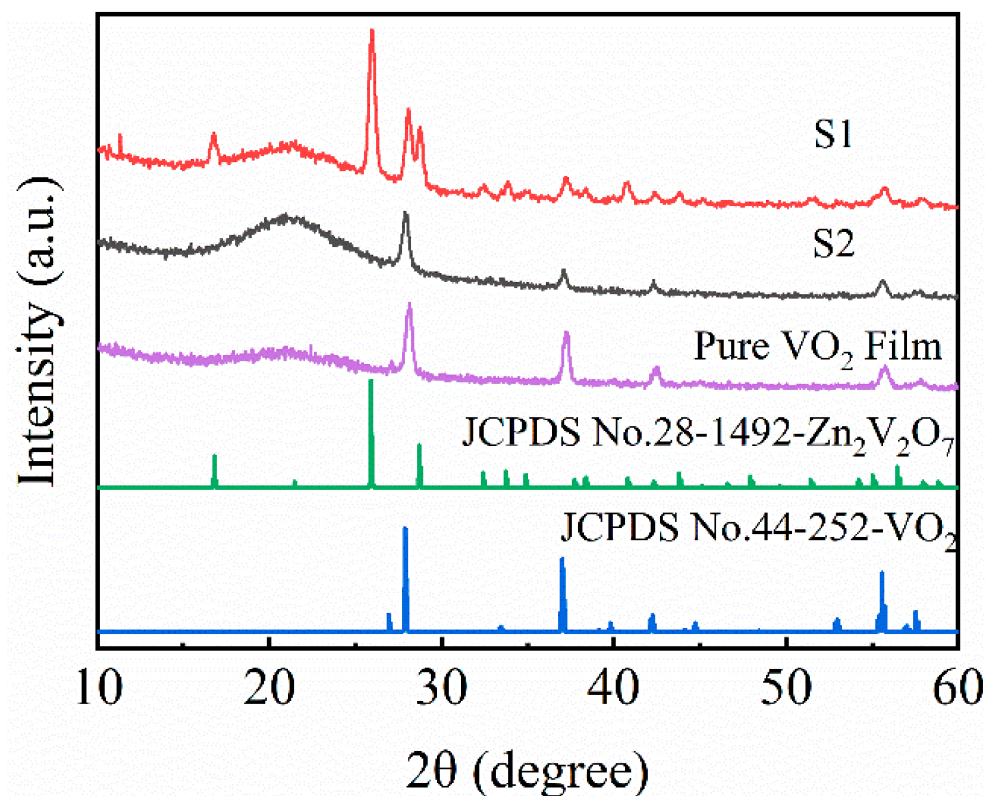


Figure 2. XRD patterns of sample S1, S2 and pure VO₂ film.

In order to further investigate the effect of acid solution treatment on the morphologies evolution of the samples, SEM and AFM test were performed on sample S1, S2 and pure VO₂ film and the results were depicted in Figure 3. It can be seen that the pure VO₂ film and sample S1 were quite dense that was comparable to the films prepare by magnetron sputtering method which was unfavorable for the optical properties. Meanwhile the color of top view of the films surface evolved from dark to bright for pure VO₂ film, sample S1

and sample S2 gradually, which means the roughness of films increased as the SEM images are morphological liner images [33], and the deduction were further confirmed by the AFM images shown in Figure 3g,h in which the root mean-square roughness (RMS) was obviously increased from 8.22 nm of sample S1 to 22.6 nm of sample S2. With introduction of $\text{Zn}_2\text{V}_2\text{O}_7$, the grains in sample S2 became less uniform. After acid solution treatment, the film was the brightest. It can be clearly seen that the porous structures between the isolated particles in the films increased significantly after acid solution treatment (Figure 3c) since the $\text{Zn}_2\text{V}_2\text{O}_7$ were removed by the acid solution. It was believed that such typical structures would benefit for improvement of T_{lum} and ΔT_{sol} simultaneously since the LSPR effect would generate. Additionally, the film thickness increased significantly from 115 nm to 194 nm for pure VO_2 film and $\text{Zn}_2\text{V}_2\text{O}_7$ - VO_2 composite film (S1) due to the generation of $\text{Zn}_2\text{V}_2\text{O}_7$ (Figure 3d–f). After acid solution treatment on sample S1, film thickness for sample S2 reduced to 124 nm that was almost identical to that of the pure VO_2 film, indicating the $\text{Zn}_2\text{V}_2\text{O}_7$ was performed as the sacrificial template to prepare the porous structures with VO_2 being isolated (Figure 3c).

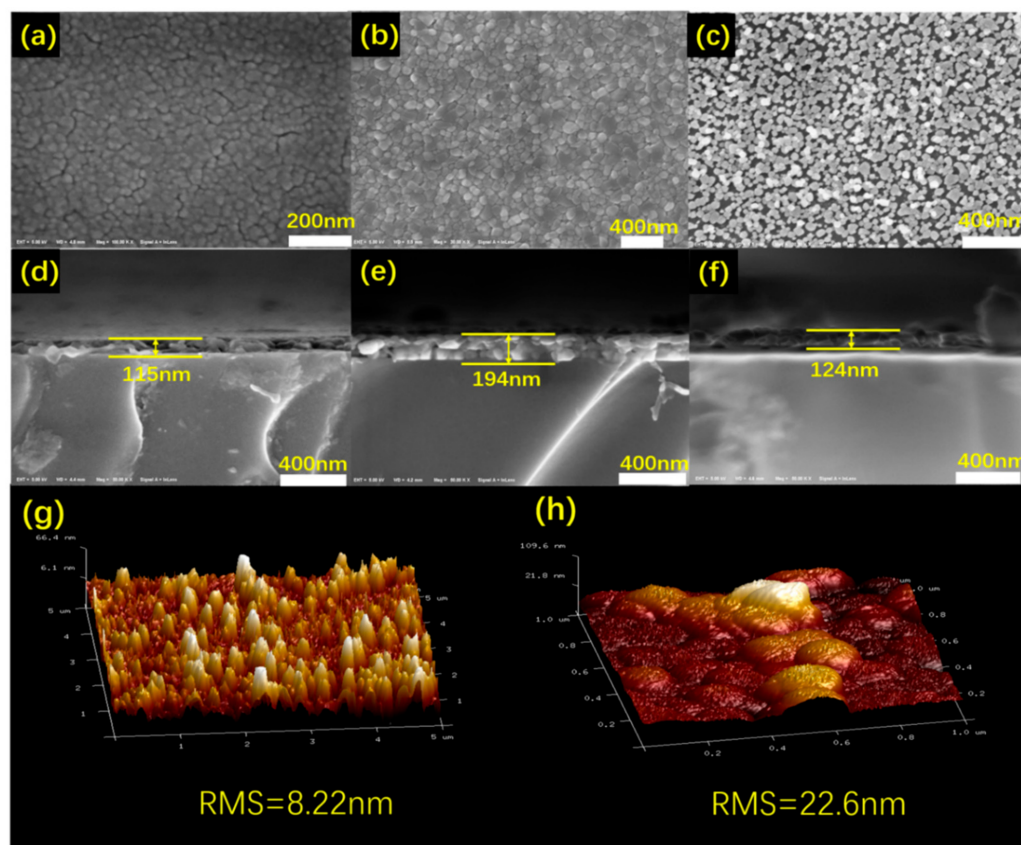


Figure 3. Top view SEM images of surface morphology of (a) pure VO_2 film, (b) sample S1 and (c) sample S2, cross-section SEM images of (d) pure VO_2 film, (e) sample S1 and (f) sample S2 and AFM images of (g) sample S1 and (h) sample S2.

In order to analyze the elemental composition in the films, XPS characterization was performed and the results are shown in Figure 4. All the core level binding energies have been calibrated by the standard C 1s binding energy of 284.8 eV. The Zn 2p peak was obviously observed in sample S1 but hardly seen in sample S2, indicating that there is a large amount of Zn in sample S1 while small amount of Zn in sample S2 (Figure 4a,b). Especially in Figure 4b, the Zn 2p core level was split into Zn 2p_{3/2} (1022.1 eV) and Zn 2p_{1/2} (1045.2 eV) peaks, indicating that Zn element in the samples existed as +2 in valence. It was demonstrated that the $\text{Zn}_2\text{V}_2\text{O}_7$ was sacrificed completely after acid solution process, which agreed well with the above XRD and SEM results. Figure 4c,d showed the high-

resolution analysis of V $2p_{3/2}$ and O 1s peaks, and the fitting curves based on Gaussian function. It can be seen that V element was mainly in a +5 valence state before acid solution process due to the formation of $Zn_2V_2O_7$ on the surface of the $Zn_2V_2O_7$ - VO_2 composite film (S1) according to the co-sputtering diagram in Figure 1a [38]. What is more, the XPS characterization could be only performed in the range of 2 nm in depth from the surface. O 1s core level (Figure 4c) was divided into two peaks that located at 529.9 and 532.1 eV, respectively. The former was assigned to the lattice oxygen in sample S1 while the latter belonged to the adsorbed oxygen species. After acid solution process was conducted in $Zn_2V_2O_7$ - VO_2 composite film, both core level peaks for V 2p and O 1s changed obviously (Figure 4d). Comparing with sample S1, core level peak at 516 eV corresponding to V^{4+} appeared with considerable intensity. Meanwhile the position of two O 1s peaks were slightly shifted, indicating that the chemical environment of O^{2-} changed, as a result, the peak located at 529.6 eV was assigned to the lattice oxygen in sample S2 and another peak at 532.5 eV was indexed to adsorbed oxygen species since more oxygen species were adsorbed on the film surface due to porous structures in sample S2 [13,15,20]. In order to conduct a more in-depth study on the composition of the $Zn_2V_2O_7$ - VO_2 composite films before and after acid solution process (sample S1 and S2), the quantitative analysis was carried out by the XPS and EDS (energy dispersive spectrometer) characterizations, and the results are shown in Table 1. It can be seen that after acid solution process, the content of Zn in the film was decreased significantly.

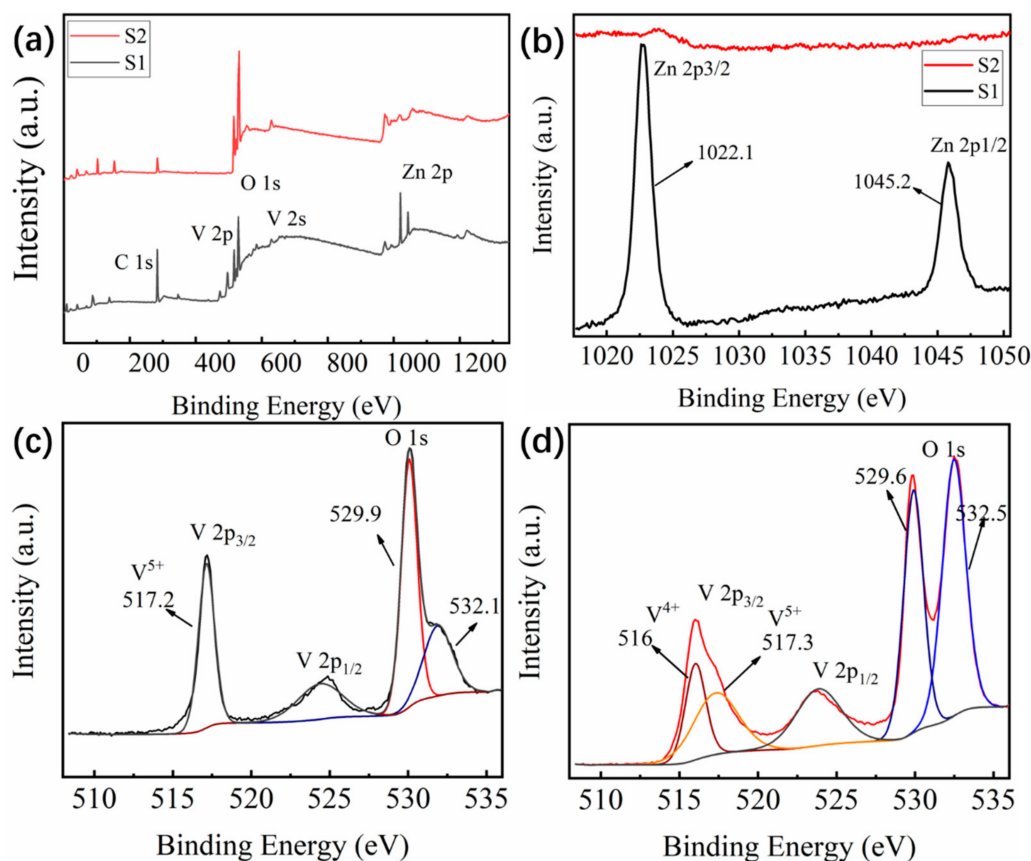


Figure 4. (a) XPS survey spectrum of samples S1 and S2, high-resolution XPS spectra for (b) Zn 2p, V 2p and O 1s core levels in (c) sample S1 and (d) sample S2.

Table 1. Elemental content of sample S1 and S2 based on the XPS and EDS results.

Element	XPS Results (at. %)		EDS Results (at. %)	
	S1	S2	S1	S2
V	30.5	35.4	19.6	7.09
Zn	11.7	0.5	14.54	0.03
O	57.8	64.1	-	-

3.2. Thermochromic Properties of VO₂ Based Films

Figure 5a showed the solar transmittance at 20 and 90 °C for sample S1, S2 and pure VO₂ film. It can be seen that the transmittance of ZnV₂O₇-VO₂ composite film (S1) and porous VO₂ film (S2) was significantly increased compared with the pure VO₂ film. For quantitative investigating the optical properties, the integrate luminous transmittance (T_{lum}) and solar modulation efficiency (ΔT_{sol}) were calculated. The ΔT_{sol} of the pure VO₂ film obtained by magnetron sputtering is 11.6%, but T_{lum} was only 31.4%. By introducing Zn₂V₂O₇ into VO₂ film, both ΔT_{sol} and T_{lum} were improved to 14.0% and 45.0% for sample S1, respectively. Such improvement was attributed to the Zn₂V₂O₇ particles dispersed in the VO₂ film which did not absorb visible light due to their higher optical band gap compared with pure VO₂ film in Figure 5b [30]. After acid solution process, the ΔT_{sol} of sample S2 was 10.7%, and the T_{lum} was as high as 72.1%, which is higher than previous reports [13–18,35–40]. The improvement in T_{lum} was probably due to the increased optical band gap induced by the reduced strain in the porous film compared with pure VO₂ and the increase porosity in the films. It can be seen from Figure 3 that the porosity of the film is significantly increased after the acid solution process, and the size of the particle was slightly reduced in Table 2, which may increase the T_{lum} of the film. In addition, after acid solution process, some VO₂ particles would be corroded, and the film become thinner, which will cause the ΔT_{sol} of the film to drop significantly. However, because the rest of the VO₂ particle size became smaller, it will lead to strong LSPR effect [33,40], resulting in the enhancement of ΔT_{sol} . Therefore, due to the influence of these two factors, the reduction of film modulation efficiency is not obvious.

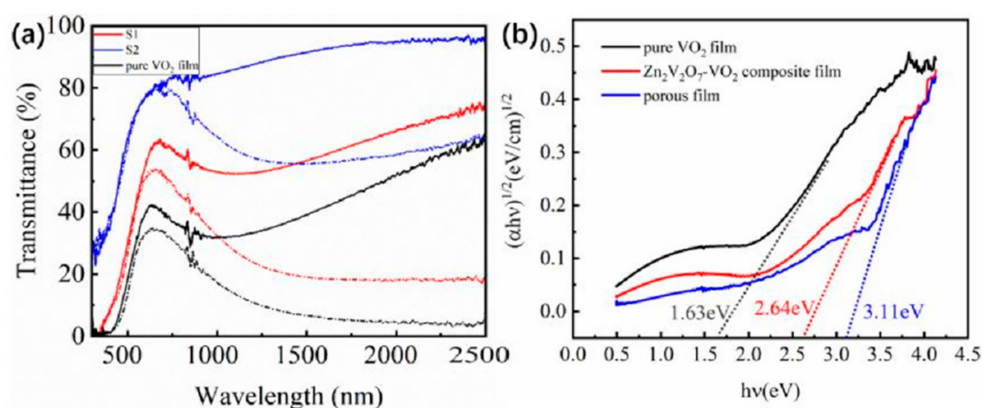


Figure 5. (a) the transmittance of sample S1, S2 and pure VO₂ film at 20 (line) and 90 °C (short point line). (b) $(\alpha h\nu)^{1/2}$ and $h\nu$ plots for VO₂, Zn₂V₂O₇-VO₂ composite film, and porous film, indicating the optical band gap of each film.

Table 2. Optical properties and grain size of $\text{Zn}_2\text{V}_2\text{O}_7\text{-VO}_2$ composite films (before acid solution processing) and porous VO_2 films (after acid solution processing) with different sputtering power of ZnO target.

Samples	Sputtering Power of ZnO Target (W)	Before Acid Solution Process V/Zn	$\text{Zn}_2\text{V}_2\text{O}_7\text{-VO}_2$ Composite Films			Porous VO_2 Films		
			Grain Size (nm)	T_{lum} (%)	ΔT_{sol} (%)	Grain Size (nm)	T_{lum} (%)	ΔT_{sol} (%)
a	60	6.1	20.3	38.9	12.5	18.6	41.0	10.0
b	90	2.3	23.4	38.1	13.0	19.0	56.4	9.2
S	120	1.4	28.1	51.8	13.7	19.5	78.0	9.9
c	150	1.7	25.6	45.0	14.0	17.5	72.1	10.7

The grain size of pure VO_2 film is 17.6 nm.

To determine the phase transition temperature (T_c) of sample S1 and S2, the resistance of the film was recorded at gradient temperatures from 20 °C to 90 °C and the results are shown in Figure 6. Here, T_c is the average between the minimum in the differential resistance ($T_{\text{heating}} + T_{\text{cooling}})/2$. The T_c is 47.5 °C, 49 °C and 64.5 °C for the pure VO_2 film, $\text{Zn}_2\text{V}_2\text{O}_7\text{-VO}_2$ composite film and porous VO_2 film, respectively. These values of T_c were higher than the critical temperature of bulk VO_2 (68 °C) because there are some strains in the obtained samples probably induced by the interface between films and substrates [35,37]. For pure VO_2 film, the interface between VO_2 particles can also leads to large strain, thus reducing the phase transition temperature. After the sacrifice of VO_2 particles and production of $\text{Zn}_2\text{V}_2\text{O}_7$ particles, the interface strain induced by particles was slightly reduced and the phase transition temperature was slightly increased to 49 °C. After the acid solution process, the interface strain between the $\text{Zn}_2\text{V}_2\text{O}_7$ and VO_2 particles was decreased obviously, hence the T_c was increased to 64.5 °C. Additionally, the hysteresis width got wider since the particle surface which was defects-enriched has been corroded, thus leading to the reduced concentration of defects.

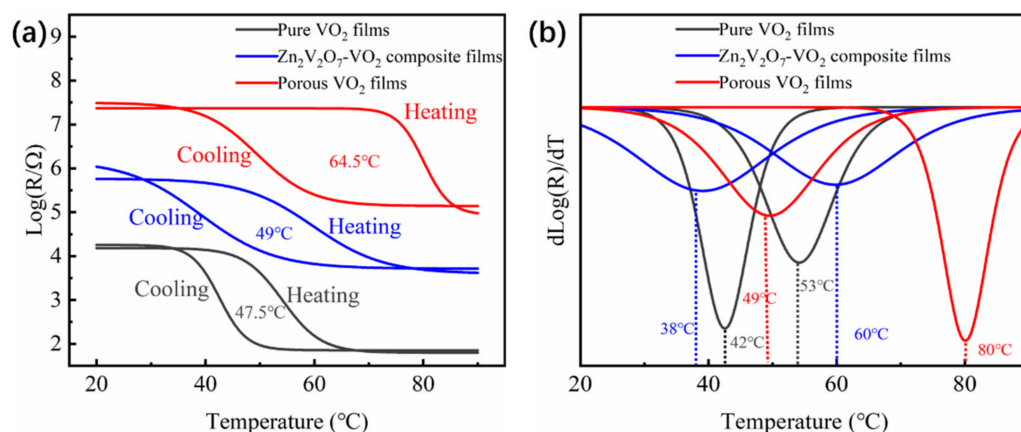


Figure 6. (a) the electrical hysteresis loop and (b) the corresponding differential for temperature of pure VO_2 film, $\text{Zn}_2\text{V}_2\text{O}_7\text{-VO}_2$ composite films and porous film.

As expected, the $\text{Zn}_2\text{V}_2\text{O}_7$ served as the sacrificial templates to generate the pores in the VO_2 films. Therefore, the content of $\text{Zn}_2\text{V}_2\text{O}_7$ was varied to evaluate the effect of porosity on the optical properties. As such, the sputtering power for ZnO target was set as 60 W, 90 W, 120 W and 150 W, respectively, to prepare $\text{Zn}_2\text{V}_2\text{O}_7\text{-VO}_2$ composite films with various $\text{Zn}_2\text{V}_2\text{O}_7$ contents, and then porous VO_2 films with different porosities were obtained by processing those composite films with acid solution in the same condition. Figure 7 shows the solar transmittance of different films. It can be seen that transmittance was obviously increased for both the $\text{Zn}_2\text{V}_2\text{O}_7\text{-VO}_2$ composite films and porous VO_2 films as increasing the sputtering power of ZnO target. The quantitative optical properties were summarized in Table 2 and comparison between them was presented in Figure 8. It was worth noting that the sputtering power of ZnO, basically, represented the content of $\text{Zn}_2\text{V}_2\text{O}_7$ since the $\text{Zn}_2\text{V}_2\text{O}_7$ was generated by the reaction of ZnO and VO_2 , but sample

S1 with sputtering power of 150 W was an exception. Comparing Zn content in both sample S1 and c1 (Figure 9), it could be found that the Zn content was decreased with increasing sputtering power from 120 W to 150 W since the Ar^+ bombarded the target material too fast when power is high enough, thus some Zn^{2+} failed to deposit on the glass substrate. Therefore, the T_{lum} of the $\text{Zn}_2\text{V}_2\text{O}_7\text{-VO}_2$ composite films and porous VO_2 films were considered to be linearly dependent on the content of $\text{Zn}_2\text{V}_2\text{O}_7$ (Figure 8b). This is also consistent with the grain size trend in Table 2. After acid solution process, the replacement of $\text{Zn}_2\text{V}_2\text{O}_7$ with pores would significantly improve the T_{lum} as the refractive index of $\text{Zn}_2\text{V}_2\text{O}_7$ is much higher than that of air, and the T_{lum} was increased by the porosity in VO_2 films. As the Zn content was increased, the grain size of the film increased slightly, but more $\text{Zn}_2\text{V}_2\text{O}_7$ was produced, leading to an enhancement of T_{lum} . The highest T_{lum} was 78% for sample c2, showing 50.6% improvement from sample c1, and for sample S1 and S2, the increment of 60.2% was obtained. The ΔT_{sol} was slightly decreased after acid solution process the $\text{Zn}_2\text{V}_2\text{O}_7\text{-VO}_2$ composite films because that the film thickness and content of VO_2 were reduced after corroding in acid solution even though the LSPR effects appeared (Figure 6b). Nevertheless, the porous film (S2) exhibited the outstanding optical performance that meets well with the needs of practical application, especially for the magnetron sputtering prepared film, and also showed an obvious advantage in the luminous transmittance compared with other thermochromic films in Table 3.

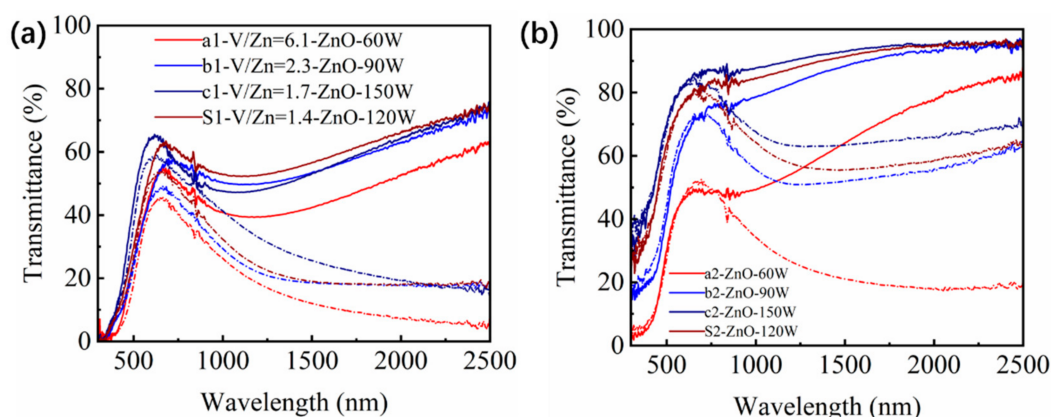


Figure 7. The transmittance of (a) $\text{Zn}_2\text{V}_2\text{O}_7\text{-VO}_2$ composite films: a1, b1, c1 and S and (b) porous VO_2 films obtained by acid solution treatment of $\text{Zn}_2\text{V}_2\text{O}_7\text{-VO}_2$ composite films: a2, b2, c2 and S2 at 20 (line) and 90 °C short point line, respectively.

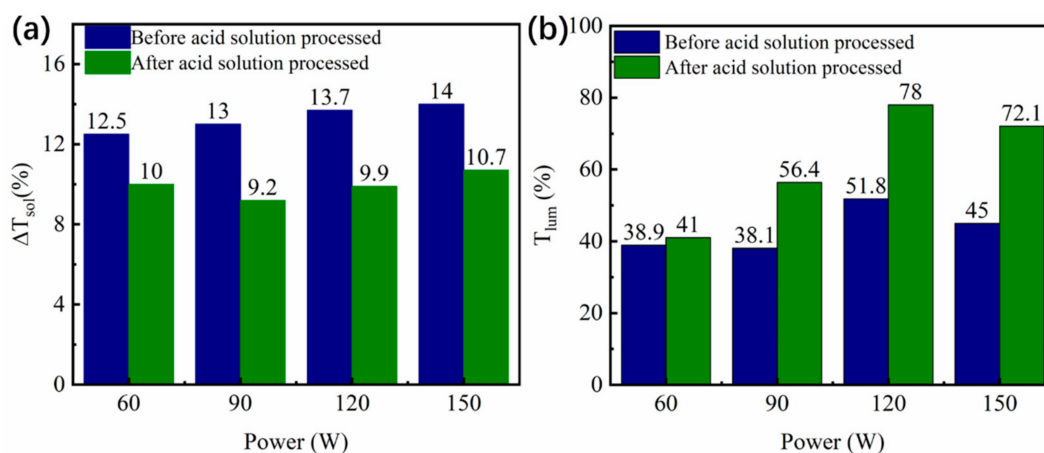


Figure 8. Comparison of (a) ΔT_{sol} and (b) T_{lum} between $\text{Zn}_2\text{V}_2\text{O}_7\text{-VO}_2$ composite films (before acid solution processing) and porous VO_2 films (after acid solution processing) with different sputtering power of ZnO target.

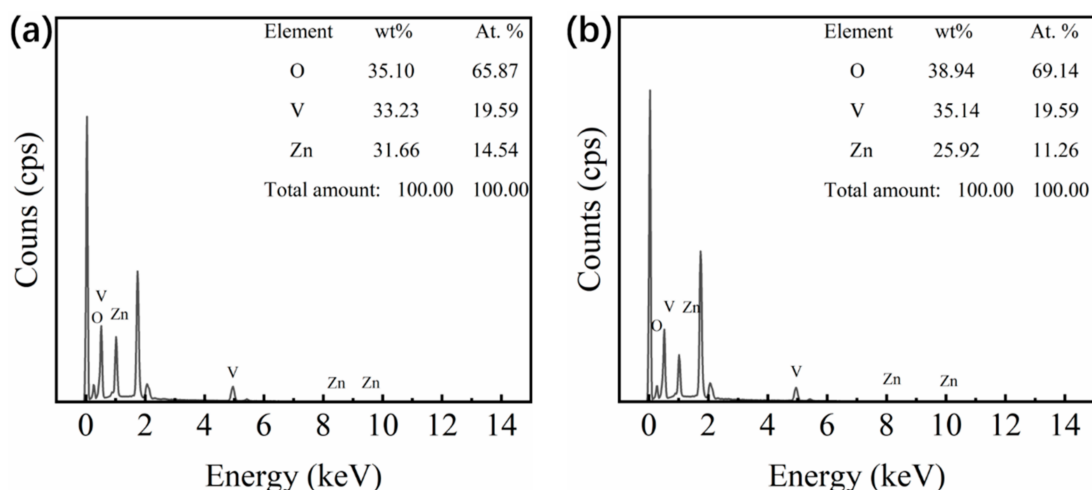


Figure 9. EDS (energy dispersive spectrometer) spectrum of (a) sample S1 and (b) sample c1 and the corresponding atomic and mass ratio for O, V and ZnO elements.

Table 3. Comparison of thermochromic performance of this work with previous works.

System	Thermochromic Properties		Reference
	T_{lum} (%)	ΔT_{sol} (%)	
Si doped VO ₂	-	9.2	Wu et al. [2]
Ni-Br-IL composite film	65.9	27.0	Chen et al. [7]
Zn-doped VO ₂	41.3	15.3	Kang et al. [13]
Mesoporous VO ₂ based film	56	12.9	Wu et al. [16]
two-dimensional nanostructure VO ₂ film	61.3	11.9	Long et al. [26]
W-doped VO ₂ film	61.7	11.7	Zhang et al. [31]
Terbium-doped VO ₂ film	54.0	8.3	Wang et al. [34]
Porous VO ₂ film	72.1	10.7	This work

"-" Means data not mentioned.

4. Conclusions

In this work, magnetron sputtering was used to prepare Zn₂V₂O₇-VO₂ composite films and the porous VO₂ films were obtained by corroding the Zn₂V₂O₇ that serve as the target sacrificial template in acid solution. Compared with processing the pure VO₂ film, this method was highly targeted, and thus leading to the controllable porous structure in VO₂ film. The porosity was linearly dependent on the content of Zn₂V₂O₇ in Zn₂V₂O₇-VO₂ composite films after acid solution process. Hence, the T_{lum} was increased significantly with the increment of content of Zn₂V₂O₇. When the ZnO sputtering power was 120 W and 150 W, the porous VO₂ films obtained by acid solution process exhibited excellent optical performance with ΔT_{sol} of 9.9% and 10.7% and T_{lum} being up to 78% and 72.1%, respectively. Therefore, the combination of these two processes is of great significance for shedding light on the modification of VO₂ films, and furthermore promoting the application of VO₂ films on energy saving smart windows.

Supplementary Materials: The following are available online at <https://www.mdpi.com/article/10.3390/ma14174927/s1>, Figure S1: XRD patterns of Zn₂V₂O₇-VO₂ composite films (before acid solution processing) and porous VO₂ films (after acid solution process) with different sputtering powers of ZnO target.

Author Contributions: Conceptualization, Z.W. and S.T.; methodology, Z.W.; software, Z.W.; validation, Z.W., B.L. (Bin Li) and S.T.; formal analysis, Z.W., B.L. (Bin Li) and S.T.; investigation, Z.W. and S.T.; resources, S.T., B.L. (Baoshun Liu), X.Z. (Xiujuan Zhao), X.Z. (Xuedong Zhou), G.T., A.P.

and S.T.; data curation, Z.W. and S.T.; writing—original draft preparation, Z.W.; writing—review and editing, Z.W., B.L. (Bin Li) and S.T.; visualization, Z.W.; supervision, B.L. (Baoshun Liu) and S.T.; project administration, S.T.; funding acquisition, S.T. All authors have read and agreed to the published version of the manuscript.

Funding: This work was supported by the National Natural Science Foundation of China (Grant No. 51772229), the 111 project (No. B18038), the National Key R&D Program of China (No. 2017YFE0192600), Key R&D Project of Hubei Province (No.2020BAB061), Open Foundation of the State Key Laboratory of Silicate Materials for Architectures at WUT (No. SYSJJ2020-04), Open Research Fund Program of Science and Technology on Aerospace Chemical Power Laboratory (No. STACPL220191B02), and State Key Laboratory of Materials Processing and Die & Mould Technology at Huazhong University of Science and Technology (No. P2021-010). We also thank the Analytical and Testing Center of WUT for the help with carrying out XRD, TEM, and FESEM analyses.

Institutional Review Board Statement: Not applicable.

Informed Consent Statement: Not applicable.

Data Availability Statement: Not applicable.

Conflicts of Interest: The authors declare no potential conflict of interest with respect to the research, authorship, and/or publication of this article.

References

1. Gao, Y.; Luo, H.; Zhang, Z.; Kang, L.; Chen, Z.; Du, J.; Minoru, K.; Cao, C. Nanoceramic VO₂ thermochromic smart glass: A review on progress in solution processing. *Nano Energy* **2012**, *1*, 221–246. [[CrossRef](#)]
2. Wu, X.; Wu, Z.; Zhang, H.; Niu, R.; He, Q.; Ji, C.; Wang, J.; Jiang, Y. Enhancement of VO₂ thermochromic properties by Si doping. *Surf. Coat. Technol.* **2015**, *276*, 248–253. [[CrossRef](#)]
3. Batista, C.; Ribeiro, R.; Carneiro, J.; Teixeira, V. DC sputtered W-doped VO₂ thermochromic thin films for smart windows with active solar control. *J. Nanosci. Nanotechnol.* **2009**, *9*, 4220–4226. [[CrossRef](#)] [[PubMed](#)]
4. Kang, L.; Gao, Y.; Luo, H.; Zhang, C.; Jin, D.; Zhang, Z. Nanoporous thermochromic VO₂ films with low optical constants, enhanced luminous transmittance and thermochromic properties. *ACS Appl. Mater. Interfaces* **2011**, *3*, 135–138. [[CrossRef](#)] [[PubMed](#)]
5. Wang, S.; Liu, M.; Kong, L.; Li, Y.; Jiang, X.; Yu, A. Recent progress in VO₂ smart coatings: Strategies to improve the thermochromic properties. *Prog. Mater. Sci.* **2016**, *81*, 1–54. [[CrossRef](#)]
6. Zhuang, B.; Dai, Z.; Pang, S.; Xu, H.; Sun, L.; Ma, F. 3D Ordered Macroporous VO₂ Thin Films with an Efficient Thermochromic Modulation Capability for Advanced Smart Windows. *Adv. Opt. Mater.* **2019**, *7*, 1900600. [[CrossRef](#)]
7. Chen, Y.; Zhu, J.; Ma, H.; Chen, L.; Li, R.; Jin, P. VO₂/Nickel-bromine-ionic liquid composite film for thermochromic application. *Sol. Energy Mater. Sol. Cells* **2019**, *196*, 124–130. [[CrossRef](#)]
8. Chen, Y.; Zeng, X.; Zhu, J.; Li, R.; Yao, H.; Cao, X.; Ji, S.; Jin, P. High Performance and Enhanced Durability of Thermochromic Films Using VO₂@ZnO Core–Shell Nanoparticles. *ACS Appl. Mater. Interfaces* **2017**, *9*, 27784–27791. [[CrossRef](#)]
9. Xu, F.; Cao, X.; Shao, Z.; Sun, G.; Long, S.; Chang, T.; Luo, H.; Jin, P. Highly Enhanced Thermochromic Performance of VO₂ Film Using “Movable” Antireflective Coatings. *ACS Appl. Mater. Interfaces* **2019**, *11*, 4712–4718. [[CrossRef](#)]
10. Kumar, M.; Singh, J.; Chae, K.; Park, J.; Lee, H. Annealing effect on phase transition and thermochromic properties of VO₂ thin films. *Superlattices Microst.* **2020**, *137*, 106335. [[CrossRef](#)]
11. Shigesato, Y.; Enomoto, M.; Odaka, H. Thermochromic VO₂ Films Deposited by RF Magnetron Sputtering Using V₂O₃ or V₂O₅ Targets. *Jpn. J. Appl. Phys.* **2000**, *39*, 6016–6024. [[CrossRef](#)]
12. Dou, S.; Wang, Y.; Zhang, X.; Tian, Y.; Hou, X.; Wang, J.; Li, X.; Zhao, J.; Li, Y. Facile preparation of double-sided VO₂ (M) films with micro-structure and enhanced thermochromic performances. *Sol. Energy Mater. Sol. Cells* **2017**, *160*, 164–173. [[CrossRef](#)]
13. Kang, J.; Liu, J.; Shi, F.; Dong, Y.; Jiang, S. The thermochromic characteristics of Zn-doped VO₂ that were prepared by the hydrothermal and post-annealing process and their polyurethane composite films. *Ceram. Int.* **2021**, *47*, 15631–15638. [[CrossRef](#)]
14. Lee, S.J.; Choi, D.S.; Kang, S.H.; Yang, W.S.; Nahm, S.; Han, S.H.; Kim, T. VO₂/WO₃-Based Hybrid Smart Windows with Thermochromic and Electrochromic Properties. *ACS Sustain. Chem. Eng.* **2019**, *7*, 7111–7117. [[CrossRef](#)]
15. Jiang, M.; Bao, S.; Cao, X.; Li, Y.; Li, S.; Zhou, H.; Luo, H.; Jin, P. Improved luminous transmittance and diminished yellow color in VO₂ energy efficient smart thin films by Zn doping. *Ceram. Int.* **2014**, *40*, 6331–6334. [[CrossRef](#)]
16. Wu, S.; Tian, S.; Liu, B.; Tao, H.; Zhao, X.; Palgrave, R.; Sankar, G.; Parkin, I. Facile synthesis of mesoporous VO₂ nanocrystals by a cotton-template method and their enhanced thermochromic properties. *Sol. Energy Mater. Sol. Cells* **2018**, *176*, 427–434. [[CrossRef](#)]
17. Long, S.; Cao, X.; Wang, Y.; Chang, T.; Li, N.; Jin, L.; Ma, L.; Xu, F.; Sun, G.; Jin, P. Karst landform-like VO₂ single layer solution: Controllable morphology and excellent optical performance for smart glazing applications. *Sol. Energy Mater. Sol. C* **2020**, *209*, 110449. [[CrossRef](#)]

18. Ke, Y.; Zhang, Q.; Wang, T.; Wang, S.; Li, N.; Lin, G.; Liu, X.; Dai, Z.; Yan, J.; Yin, J.; et al. Cephalopod-inspired versatile design based on plasmonic VO₂ nanoparticle for energy-efficient mechano-thermochromic windows. *Nano Energy* **2020**, *73*, 104785. [[CrossRef](#)]
19. Li, B.; Tian, S.; Tao, H.; Zhao, X. Tungsten doped M-phase VO₂ mesoporous nanocrystals with enhanced comprehensive thermochromic properties for smart windows. *Ceram. Int.* **2019**, *45*, 4342–4350. [[CrossRef](#)]
20. Zou, Z.; Zhang, Z.; Xu, J.; Yu, Z.; Cheng, M.; Xiong, R.; Lu, Z.; Liu, Y.; Shi, J. Thermochromic, threshold switching, and optical properties of Cr-doped VO₂ thin films. *J. Alloy. Compd.* **2019**, *806*, 310–315. [[CrossRef](#)]
21. Li, B.; Liu, J.; Tian, S.; Liu, B.; Yang, X.; Yu, Z.; Zhao, X. VO₂-ZnO composite films with enhanced thermochromic properties for smart windows. *Ceram. Int.* **2020**, *46*, 2758–2763. [[CrossRef](#)]
22. Li, B.; Yao, J.; Tian, S.; Fang, Z.; Wu, S.; Liu, B.; Gong, X.; Tao, H.; Zhao, X. A facile one-step annealing route to prepare thermochromic W doped VO₂ (M) particles for smart windows. *Ceram. Int.* **2020**, *46*, 18274–18280. [[CrossRef](#)]
23. Chen, H.-W.; Li, C.-I.; Ma, C.-H.; Chu, Y.-H.; Liu, H.-L. Strain engineering of optical properties in transparent VO₂/muscovite heterostructures. *Phys. Chem. Chem. Phys.* **2021**, *23*, 8908–8915. [[CrossRef](#)]
24. D'Elia, A.; Grazioli, C.; Cossaro, A.; Li, B.; Zou, C.; Rezvani, S.; Pinto, N.; Marcelli, A.; Coreno, M. Strain mediated Filling Control nature of the Metal-Insulator Transition of VO₂ and electron correlation effects in nanostructured films. *Appl. Surf. Sci.* **2021**, *540*, 148341. [[CrossRef](#)]
25. Nazari, M.; Zhao, Y.; Kuryatkov, V.V.; Fan, Z.Y.; Bernussi, A.A.; Holtz, M. Temperature dependence of the optical properties of VO₂ deposited on sapphire with different orientations. *Phys. Rev. B* **2013**, *87*, 035142. [[CrossRef](#)]
26. Ke, Y.; Wen, X.; Zhao, D.; Che, R.; Xiong, Q.; Long, Y. Controllable Fabrication of Two-Dimensional Patterned VO₂ Nanoparticle, Nanodome, and Nanonet Arrays with Tunable Temperature-Dependent Localized Surface Plasmon Resonance. *ACS Nano* **2018**, *11*, 7542–7551. [[CrossRef](#)]
27. Sol, C.; Portnoi, M.; Li, T.; Gurunatha, K.; Schläfer, J.; Guldin, S.; Parkin, I.; Papakonstantinou, I. High-performance planar thin film thermochromic window via dynamic optical impedance matching. *ACS Appl. Mater. Interfaces* **2020**, *12*, 8140–8145. [[CrossRef](#)]
28. Batista, C.; Ribeiro, R.M.; Teixeira, V. Synthesis and characterization of VO₂-based thermochromic thin films for energy-efficient windows. *Nanoscale Res. Lett.* **2011**, *6*, 301. [[CrossRef](#)]
29. Riapanitra, A.; Asakura, Y.; Yin, S. One-step hydrothermal synthesis and thermochromic properties of chlorine-doped VO₂(M) for smart window application. *Funct. Mater. Lett.* **2020**, *13*, 1951008. [[CrossRef](#)]
30. Zhang, Y.; Li, B.; Wang, Z.; Tian, S.; Liu, B.; Zhao, X.; Li, N.; Sankar, G.; Wang, S. Facile Preparation of Zn₂V₂O₇-VO₂ Composite Films with Enhanced Thermochromic Properties for Smart Windows. *ACS Appl. Electron. Mater.* **2021**, *3*, 2224–2232. [[CrossRef](#)]
31. Zhang, L.; Xia, F.; Yao, J.; Zhu, T.; Xia, H.; Yang, G.; Liu, B.; Gao, Y. Facile synthesis, formation mechanism and thermochromic properties of W-doped VO₂(M) nanoparticles for smart window applications. *J. Mater. Chem. C* **2020**, *8*, 13396–13404. [[CrossRef](#)]
32. Gonçalves, A.; Resende, J.; Marques, A.; Pinto, J.V.; Nunes, D.; Marie, A.; Pereira, L.; Martins, R.; Fortunato, E. Smart optically active VO₂ nanostructured layers applied in roof-type ceramic tiles for energy efficiency. *Sol. Energy Mater. Sol. Cells* **2016**, *150*, 1–9. [[CrossRef](#)]
33. Liang, J.; Guo, J.; Zhao, Y.; Su, T.; Zhang, Y. The effects of surface plasmon resonance coupling effect on the solar energy modulation under high transmittance of VO₂ nanostructure. *Sol. Energy Mater. Sol. C.* **2019**, *199*, 1–7. [[CrossRef](#)]
34. Wang, N.; Duchamp, M.; Dunin-Borkowski, R.; Liu, S.; Zeng, X.; Cao, X.; Long, Y. Terbium-Doped VO₂ Thin Films: Reduced Phase Transition Temperature and Largely Enhanced Luminous Transmittance. *Langmuir* **2016**, *32*, 759–764. [[CrossRef](#)] [[PubMed](#)]
35. Xu, F.; Cao, X.; Luo, H.; Jin, P. Recent advances in VO₂-based thermochromic composites for smart windows. *J. Mater. Chem. C* **2018**, *6*, 1903–1919. [[CrossRef](#)]
36. Li, Y.; Ji, S.; Gao, Y.; Luo, H.; Kanehira, M. Core-shell VO₂@TO₂ nanorods that combine thermochromic and photocatalytic properties for application as energy-saving smart coatings. *Sci. Rep.* **2013**, *3*, 1370. [[CrossRef](#)]
37. Morin, F.J. Oxides Which Show a Metal-to-Insulator Transition at the Neel Temperature. *Phys. Rev. Lett.* **1959**, *3*, 34–36. [[CrossRef](#)]
38. Miyazaki, H.; Yasui, I. Substrate bias effect on the fabrication of thermochromic VO₂ films by reactive RF sputtering. *J. Phys. D Appl. Phys.* **2006**, *39*, 2220–2223. [[CrossRef](#)]
39. Gagaoudakis, E.; Aperathitis, E.; Michail, G.; Kiriakidis, G.; Binas, V. Sputtered VO₂ coatings on commercial glass substrates for smart glazing applications. *Sol. Energy Mater. Sol. Cells* **2021**, *220*, 110845. [[CrossRef](#)]
40. Long, S.; Cao, X.; Huang, R.; Xu, F.; Li, N.; Huang, A.; Sun, G.; Bao, S.; Luo, H.; Jin, P. Self-Template Synthesis of Nanoporous VO₂-Based Films: Localized Surface Plasmon Resonance and Enhanced Optical Performance for Solar Glazing Application. *ACS Appl. Mater. Interfaces* **2019**, *11*, 22692–22702. [[CrossRef](#)]